FRACTURE TOUGHNESS AND MICROSTRUCTURE IN AA 2XXX ALUMINIUM ALLOYS

[1]E. Gariboldi, [1]D. Ripamonti, [1]L. Signorelli, [1]G. Vimercati, [2]F. Casaro

[1] Politecnico di Milano, Dipartimento di Meccanica, Milano (MI)

[2] Varian Vacuum Technologies, Leinì (TO)

Abstract

The paper presents the toughness properties of forgings made of two AA 2xxx series aluminium alloys with different microstructural conditions. Fracture toughness tests in crack opening mode I were performed on compact tension specimens machined from the forgings in different orientations. The tests were performed both at room temperature and at 130°C.

Fracture toughness properties were related to microstructural and fractographic features of the alloys in order to discuss on their failure mechanisms. The effect of the coarse intermetallic phases within grains or at their boundaries in the different conditions was underlined. The testing temperature, within the range here investigated, neither affected fracture toughness properties nor failure mechanisms.

Riassunto

Il lavoro illustra le proprietà di tenacità alla frattura misurate in forgiati di grandi dimensioni realizzati con due leghe di alluminio della serie 2xxx in differenti condizioni microstrutturali. Dai forgiati sono stati ricavati provini CT con differenti orientazioni sui quali sono state condotte prove di tenacità a frattura secondo il modo I di apertura della cricca. Le proprietà ottenute sono state correlate con la microstruttura riscontrata nei campioni e completate con analisi frattografiche atte ad individuare i meccanismi di cedimento. È stato così messo in luce l'effetto delle diverse microstrutture ed in particolare delle particelle grossolane di fasi intermetalliche presenti a bordo grano o all'interno dei grani che differenziano i forgiati nelle leghe esaminate di composizione più complessa.

KEYWORDS

Al alloy AA2014, Al alloy AA2618, fracture toughness, microstructure.

1. INTRODUCTION

Aluminium-alloy forging is currently used to manufacture structural components of relatively large and complex shape. The plastic deformation imparted to the material can positively affect its microstructure by promoting recrystallization cycles and a greater homogeneity of alloying elements. However, it should be considered that in large size forgings, the relatively low amount of plastic strain given to the alloy cannot completely refine the structure and intermetallic particles as in other small-size wrought products such as extruded bars or rolled sheets. In addition, the slower quenching rates experienced by large forgings result in lower mechanical properties achieved after the subsequent aging process. Large differences in cooling rate between surface and centre of large forgings during solution annealing also result in remarkable residual stresses, that are often relieved by inserting a plastic deformation step after quenching and before the aging treatment [1]. This method also modifies the precipitation sequence and kinetics of the alloy. The above described effects significantly affect the tensile and fracture properties of aluminium alloy forgings. Focusing the attention on the fracture of aluminium alloys, it was reported that toughness is strictly related to the presence of coarse particles, 0.1 to 10 μm in diameter, that can be either non-equilibrium particles formed during solidification or inclusions from insoluble impurities [2]. These particles crack easily as the matrix deforms within the plastic flow zone at the crack tip and causes the typical ductile fracture mode where crack propagates via coalescence of voids. The amount, size and distribution of these second phase particles is thus relevant for the fracture toughness properties and even material with comparable tensile properties can display significantly different fracture toughness properties.

In addition to the abovementioned effect, the role played by submicrometer particles (0.01 to 0.5 μm in diameter) need to be considered. In the case of the same volume fraction and microstructural features of coarse particles, a substantial modification of toughness can be observed in age hardenable aluminium alloys varying the amount and characteristics of fine hardening particles. The behaviour is complex and the fine hardening particles are responsible for it. It is well known that the presence of particle having suitable distribution and size enhances the resistance of peak aged alloys to deformation and thus tends to reduce the extension of the plastic zone, positively affecting toughness [2, 3]. On the other hand, the lower strain-hardening capacity of the material in the peak aged condition with respect to the underaged condition, also gives rise to local plastic instabilities that significantly contribute to reduce the material toughness [2]. Further, where grain boundary precipitate free zones are observed, strain localization in these regions and intergranular ductile fracture can occur [3, 4]. In these cases the fracture toughness depends on the spacing and size of the void-nucleating particles at grain boundaries [4, 5]. The higher fracture toughness displayed by alloys in the underaged with respect to over-aged condition as well as the transition towards intergranular ductile fracture mode as overaging proceeds confirm this latter effect [2, 4].

The aim of the present paper is to contribute to a better understanding of the correlation between microstructure, tensile and toughness properties of aluminium forgings as a result of different thermomechanical cycles, focusing in particular to the role of large second phase particles.

2. MATERIALS INVESTIGATED

The present investigation was carried out on three forgings having a roughly cylindrical shape with a diameter of 250 mm, made of aluminium alloys AA2014 (Al4CuSiMg) and AA2618 (Al2Cu1.5MgNi). The parts had been forged from extruded bars of diameter 190 mm with different manufacturing cycles.

Two forged samples of the AA2014 alloy were produced by forging in two steps at 390°C. The samples were then heat treated to T6 temper by different parameters. A first sample, hereafter referred to as 2014-A forging was solution annealed at 505°C for 6 hours, water quenched and artificially aged at 160°C for 14 hours, following the usual industrial heat treatment route. In the case of the forging in AA2618 alloy (hereafter referred to as 2618 forging), the solution annealing at the usual temperature for this material, 530°C, lasted 1 hour, and it was followed by water quenching and by artificial aging at 190°C for 20 hours, following a common industrial practice. The 2014-B forging was produced and heat treated as for 2618 material, leading to a substantially overaged matrix and to intermetallic phases distribution rather different than that of 2014-A forging.

Light optical microscopy observations and Vickers hardness tests (0.98N load) were performed to evaluate the general microstructural features. Tensile test specimens were machined from the forgings in the hoop direction in regions characterized by a homogeneous structure and hardness.

Two sets of Compact Tension (CT) fracture toughness specimens were machined with cracks laying in diametral planes of the forgings. In the first set, the crack propagation direction was radial (CR direction according to ASTM E399-90 and B645-02 [6, 7]) while in the second set it was longitudinal (CL direction). The specimens had a thickness B of 20 mm [6, 7].

Tests were carried out on a MTS 810 universal testing machine, equipped with an environmental chamber suitable for test temperatures up to 250°C. Before fracture toughness tests, a precracking stage was performed at test temperature until a total crack length (machined notch and fatigue crack) of about 20 mm was reached. Precracking was performed under load control (sinusoidal cycles at 10 Hz frequency) while crack length was monitored via the elastic compliance technique by measuring the Crack Opening Displacement (COD). The stress intensity factor during pre-cracking decreased linearly with crack length from 11 to 8 MPa•m$^{1/2}$. Fracture

toughness tests were carried out imposing a displacement rate of 0,025 mm/s, monitoring the COD and applied load until the occurrence of unstable crack propagation.

In a second stage of the research study, the toughness of the materials at 130°C was investigated. The J_{IC} integral was measured according to the single-specimen technique and the ASTM E1820-01 standard [8]. The J_{IC} parameter was evaluated instead of K_{IC} since the material toughness was expected to be greater than that measured at room temperature. The tests were performed monitoring crack length via the compliance method at fixed steps of COD. In order to reduce the strain accumulated under load during each load step due to creep effects at 130°C, the holding period under constant applied load (P) for the adjustment of the crack length was fixed to 1 s. J_Q was estimated according to the mentioned standard as the intercept between the power-law curve (fitting the experimental data within the range stated by ASTM E1820-01) and the straight line passing to the

point Δa = 0.2 mm, P = 0 N with a slope corresponding to a double flow stress (this latter corresponding to the average between the yield and the ultimate tensile stress).

Validity requirements of J_{IC} tests were not met in all cases since unstable crack propagation or pop-in phenomena occurred in some samples. In these cases the K_Q parameter was evaluated from the P-COD curves.

Fracture surfaces were observed by scanning electron microscopy (SEM). Metallographic sections were also cut perpendicularly to the crack plane to observe the crack propagation path by optical microscopy and SEM.

3. RESULTS

3.1 MICROSTRUCTURE

All forgings were characterized by grains elongated along the main plastic flow path experienced during forging. Coarse intermetallic particles were also present in the microstructure, as expected for these alloys. More specifically, the 2014-A material (figure 1a) was characterized by elongated grains with a transversal size of about 50 μm and by large intermetallic particles aligned in the flow direction: globular Al_2Cu (θ) particles (bright particles in figure 1a) and blocky shaped clustered particles containing Fe, Mn, Si and Cu (darker particles in the same figure). In regions where these particles were observed small equiaxed grains were often detected

suggesting the local recrystallization effect induced by these intermetallics.

The direction of plastic flow was less evident in the 2014-B samples, that displayed rather elongated grains of 50-100 μm in transverse size together with smaller equiaxed grains in the regions containing large intermetallic particles (figure 1b). These were in lower amount with respect to the previous alloy. Particles with dark appearance at grain boundaries (figure 1b) were of complex chemical composition. On the contrary globular Al_2Cu particles had a bright appearance in
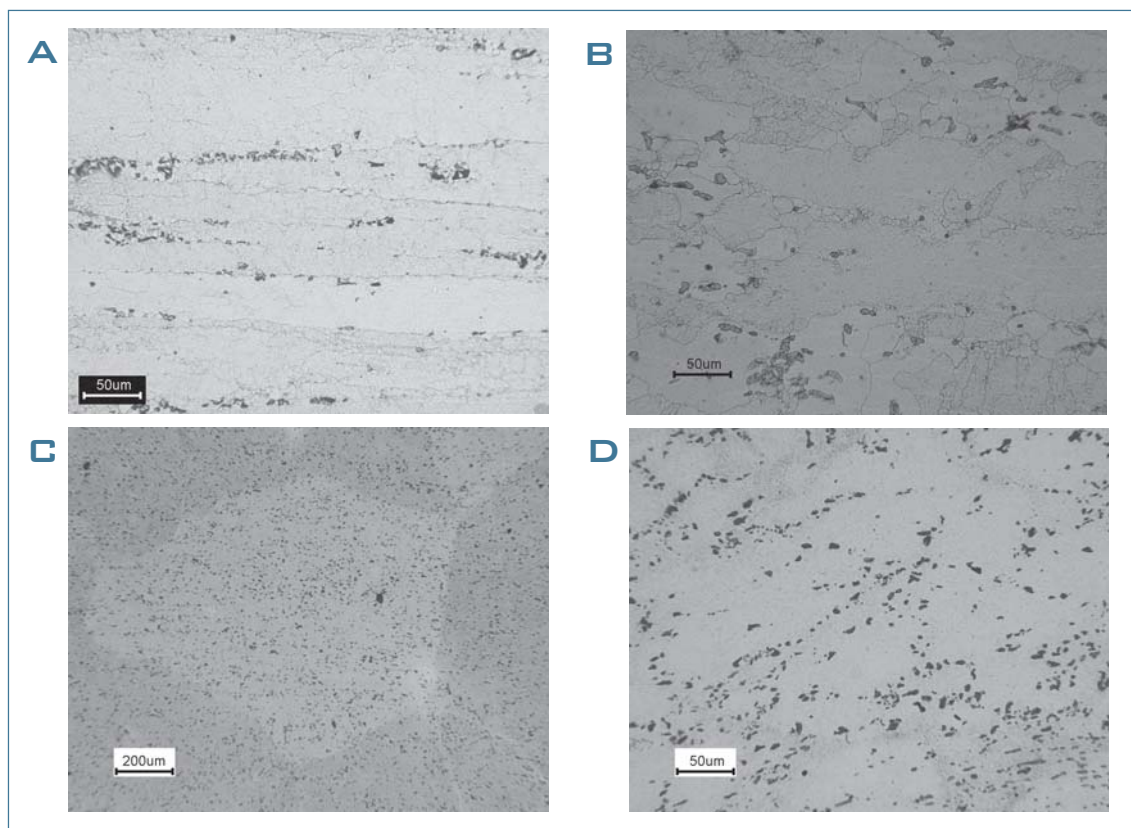

Fig. 1:
Typical microstructure of the investigated forgings. 2014-A (a), 2014-B (b), 2618 at low (c) and higher (d) magnification. The longitudinal axis of forgings is horizontal in all the micrographs.

micrographs and were observed both inter- and intragranularly.

The 2618 sample was characterized by very large grains slightly elongated in the flow direction. Their size in the transverse direction was of the order of 500 μm, as shown in figure 1c. As expected, considering the composition of the AA2618 alloy [1], several intragranular FeNiAl$_9$ particles were observed together with globular Al$_2$Cu and (CuFe) Al$_3$ precipitates.

The microstructure and hardness of the forgings were in all cases homogeneous in the regions where tension and toughness specimens were sampled.

3.2 MECHANICAL BEHAVIOUR

The average tensile properties in hoop direction of the investigated materials at room temperature and at 130°C are summarized in Table I. At room temperature, the 2014-A forging showed the highest tensile strength and the lowest ductility. The increase in test temperature from 20 to 130°C led to a significant reduction in the ultimate tensile strength (UTS) and 0,2% proof stress (YS) and to a corresponding significant increase in reduction of area (Z) and elongation (A) at fracture.

The results of the fracture toughness tests are summarized in Table 2 while representative load vs. COD graphs are shown in Figure 2. Here, the lines needed for the evaluation of K$_Q$ are added

to the experimental curves

The condition of plain strain crack propagation in CT specimen fracture can be met for sufficiently large specimens. The minimum specimen thickness
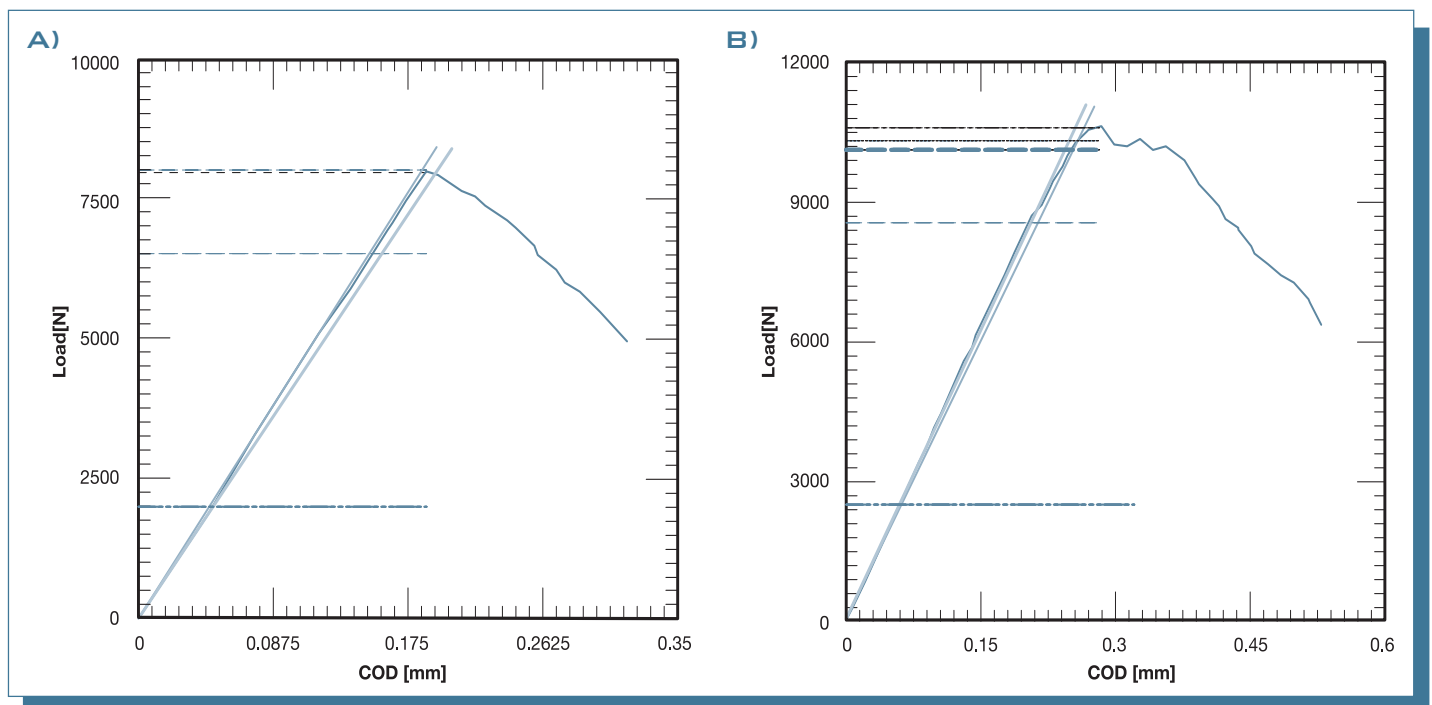
Table 1: Tensile properties of the investigated alloys

	YS [MPa]		UTS [MPa]		A [%]		Z [%]	
Temperature	20°C	130°C	20°C	130°C	20°C	130°C	20°C	130°C
2014-A	421	386	454	402	1,8	9,3	3,7	15,8
2014-B	357	341	425	393	7,3	8,4	14,2	16,9
2618	350	345	416	409	6,4	8,6	10,8	12,3

Table 2: Fracture toughness of the materials investigated (K$_Q$ or K$_{IC}$ according to ASTM B645 and K$_{JIC}$ according to ASTM E1820)

Specimen direction	Temperature [°C]	2014-A MPa·m$^\Omega$	2014-B MPa·m$^\Omega$	2618 MPa·m$^\Omega$
CL	20	19,3 (K$_{IC}$)	23,0 (K$_Q$)	22,4 (K$_Q$)
CL	20	20,1 (K$_{IC}$)	24,9 (K$_Q$)	23,3 (K$_Q$)
Average CL	20	19,7 (K$_{IC}$)	24,0 (K$_Q$)	22,9 (K$_Q$)
CL	130	18,8 (K$_{IC}$)	23,4 (K$_{JIC}$)	21,9 (K$_Q$)
CR	20	23,4 (K$_{IC}$)	24,8 (K$_Q$)	26,9 (K$_Q$)
CR	20	22,8 (K$_{IC}$)	24,4 (K$_Q$)	26,7 (K$_Q$)
Average CR	20	23,1 (K$_{IC}$)	24,6 (K$_Q$)	26,8 (K$_Q$)
CR	130	21,4 (K$_{JIC}$)	23,4 (K$_{JIC}$)	25,6 (K$_Q$)

Fig. 2: Load vs. COD plots of the samples tested at 20°C.
A) 2014-A forging, CL specimen; B) 2014-B forging, CR specimen

Specimen direction	Temperature [°C]	2014-A	2014-B	2618
CL	20	9.4	4.8	4.9
CL	20	8.7	4.1	4.5
Average CL	20	9.1	4.5	4.7
CL	130	9.1	4.2	4.9
CR	20	6.4	4.1	3.4
CR	20	6.8	4.3	3.4
Average CR	20	6.6	4.2	3.4
CR	130	7.4	3.3	3.6

TABLE 4: J_{IC} VALUES (N/MM) OF THE INVESTIGATED
FORGINGS TESTED AT 130°C

Specimen direction	Temperature [°C]	2014-A [N/mm]	2014-B [N/mm]	2618 [N/mm]
CL	130	-	7.23	-
CR	130	5.96	7.00	-

(B) to be adopted can be calculated, at the end of the tests, according to the two standard above considered:

$$B_{min} = 5 \cdot (K_Q/YS)^2 \qquad \text{according to ASTM B645} \qquad (1)$$

$$B_{min} = 2{,}5 \cdot (K_Q/YS)^2 \qquad \text{according to ASTM E399} \qquad (2)$$

Thus, the minimum thickness required by the E399 standard is half of that required by the B645 standard for aluminium alloys. The agreement to plain strain conditions and the possible deviation from the minimum value of B can be evaluated using a parameter F, defined as:

$$F = B \cdot (YS/K_Q)^2 \qquad (3)$$

Where F greater than 5 means that the requirements for plain strain condition are met for both standards and valid K_{IC} can be obtained. 2,5<F<5 means that plain strain condition was met only according to ASTM E399, while F lower than 2,5 means that according for both standard the plain strain condition was not obtained.

It can be observed that F was greater than 5 for all the tests carried out on the 2014-A samples, while for the other two alloys F laid in the range 3,3 to 4,9. Even though the requirement on specimen thickness did not allowed to equate K_Q to K_{IC} according to ASTM B645 standard, for specimen where F was not far from 5 it can be reasonably assumed that plane strain condition was not far to be reached. For the same reason and for comparison purposes fracture toughness test results at room temperature were reported in Table 2.

Tests performed at 130°C supplied valid J_{IC} values only for the 2014-A and 2014-B samples, in the former case only in CR specimen orientation, as shown in Table 4. Figure 3a shows an example of the J-Δa curve, from which J_Q was evaluated
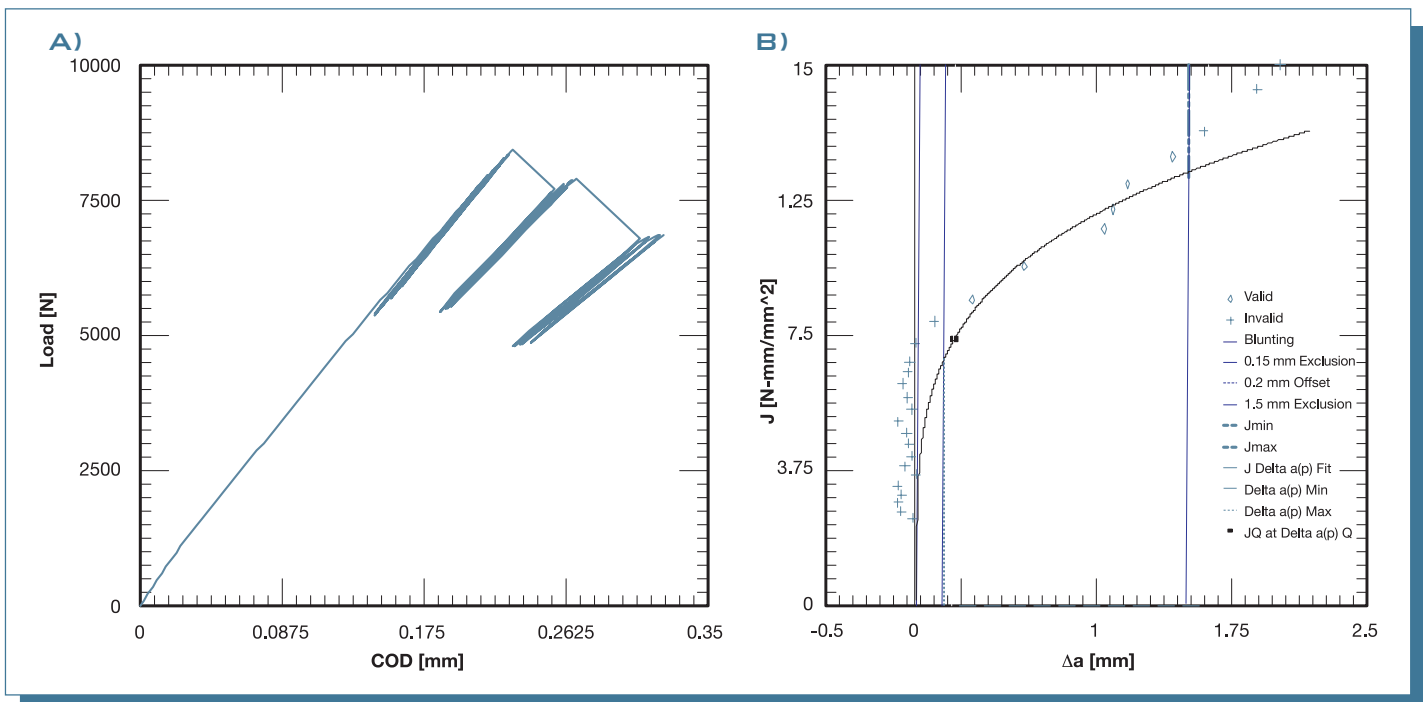

Fig. 2: Load vs. COD plots of the samples tested at 20°C.
A) 2014-A forging, CL specimen; B) 2014-B forging, CR specimen

according to the ASTM E1820 standard. As far as the AA2618 alloy that resulted to be the toughest material at room temperature, at 130°C it showed unstable crack propagation (Figure 3b) that prevented the evaluation of J_{IC}. In the cases of valid J_{IC}, K_{JIC} was computed, assuming plain strain conditions, by using the following correlation proposed by ASTM E1820 standard:

$$K_{JIC} = [(E/(1-v^2)) \cdot J_{IC}]^{0.5} \qquad (4)$$

K_{JIC} values are also listed in Table 2 for comparison purpose. Examination of this table clearly shows that toughness of 2014-B forging is greater than that of the same alloy in forging 2014-A. Further, it can be stated that in all the examined samples, crack propagation in CL orientation is favoured with respect to that in CR orientation.

3.3. FRACTOGRAPHIC OBSERVATIONS

Fractographic observations were performed at two main locations on fracture surface of each specimen in the crack propagation region: the first next to, the latter at 4 mm from the boundary with fatigue precrack. Selected images at low magnification of the first location for the different alloys and specimen orientation are reported in figure 4. In the unstable crack propagation region, the 2014-A forging showed the typical features of ductile fracture, generated by nucleation of dimples mainly from the coarser intermetallic particles fractured in a brittle way (figure 5a). Within the matrix, regions with dimples of far smaller size were also visible, laying on well-defined planes

(figure 5b). These can be correlated to the presence of fine particles that in some cases were observed inside the dimples in high magnification images that suggest ductile intergranular fracture.

The fracture surfaces of the 2014-B forging did not show significant differences from 2014-A material, with relatively extended regions of microdimples (figure 7a) that could be correlated to the presence of coarse grain boundary particles (figure 6b). The size and distribution of these particles corresponded to those observed at grain boundaries (figure 4c). The 2618 forging, showed a transgranular ductile fracture mode (figures 4d, 7b). Dimples observed on fracture surfaces nucleated from the homogeneously distributed $FeNiAl_9$ particles (figures 6c and 6d).

The fracture surfaces of specimens tested at 130°C of forgings made of AA2014 alloy were similar to those tested at room temperatures (figure 8a). On the contrary, as the temperature increased, small-size microdimples were observed on the fracture surface of the forging made of AA2618 alloy (compare figure 7b and 8b).
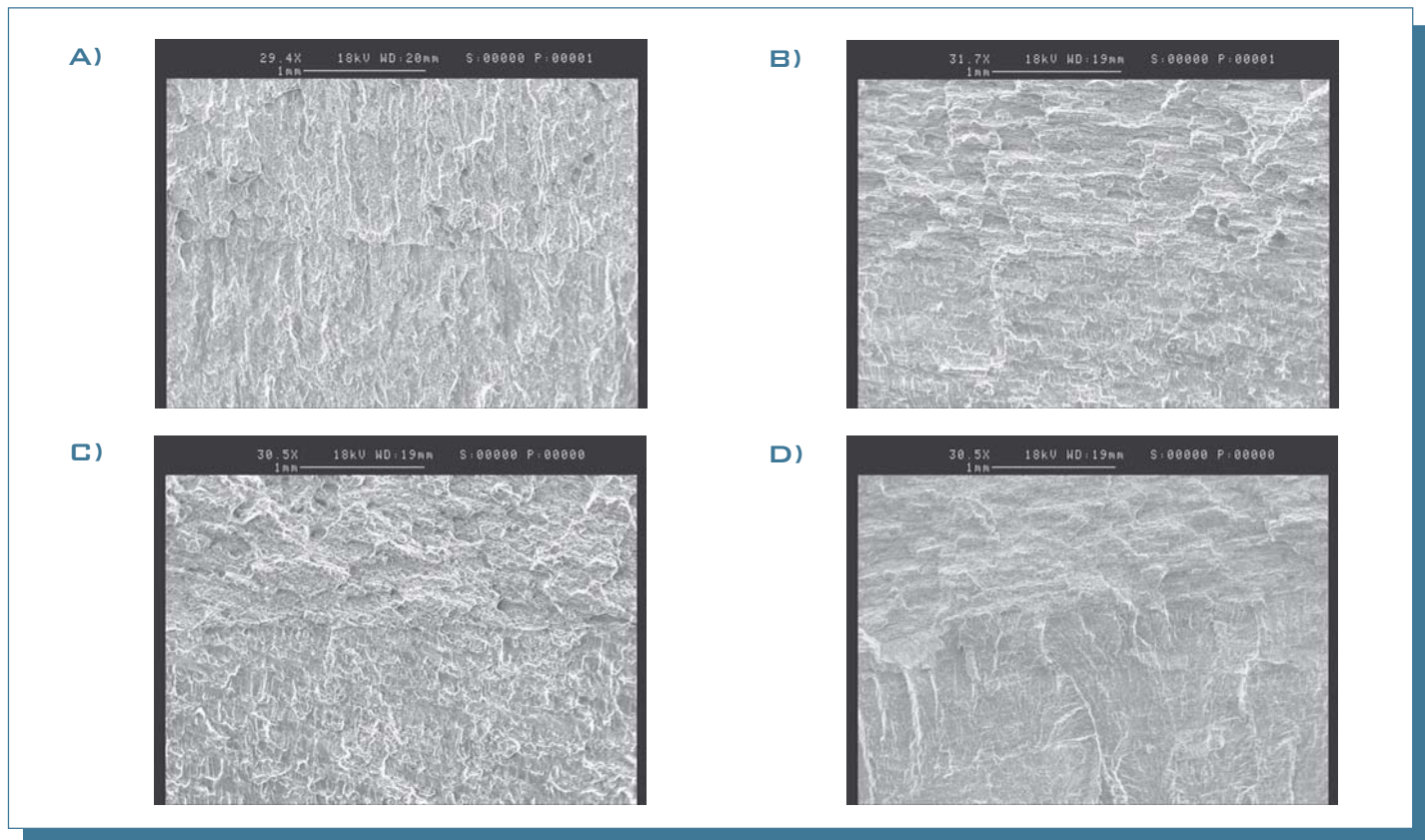

Fig. 4: Fracture surface of cracks propagated at room temperature in the boundary region between fatigue precracking and unstable crack propagation region. 2014-A forging, CL (a) and CR (b) directions. 2014-B forging; CR direction (c) and 2618, CR direction (d).
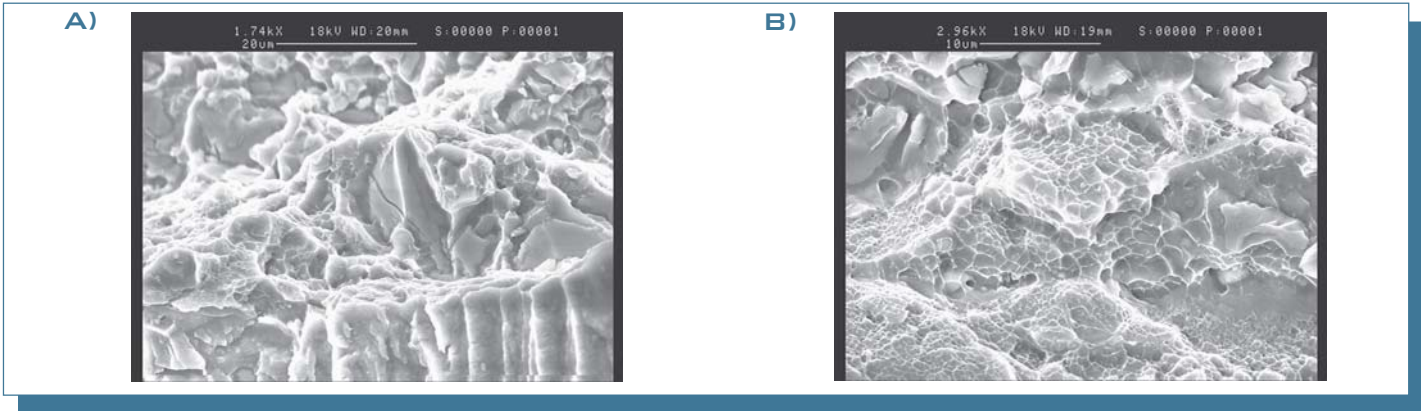
Fig. 5: Fracture surface of cracks propagating at room temperature in 2014-A forging in CL (a) and CR (b) direction.
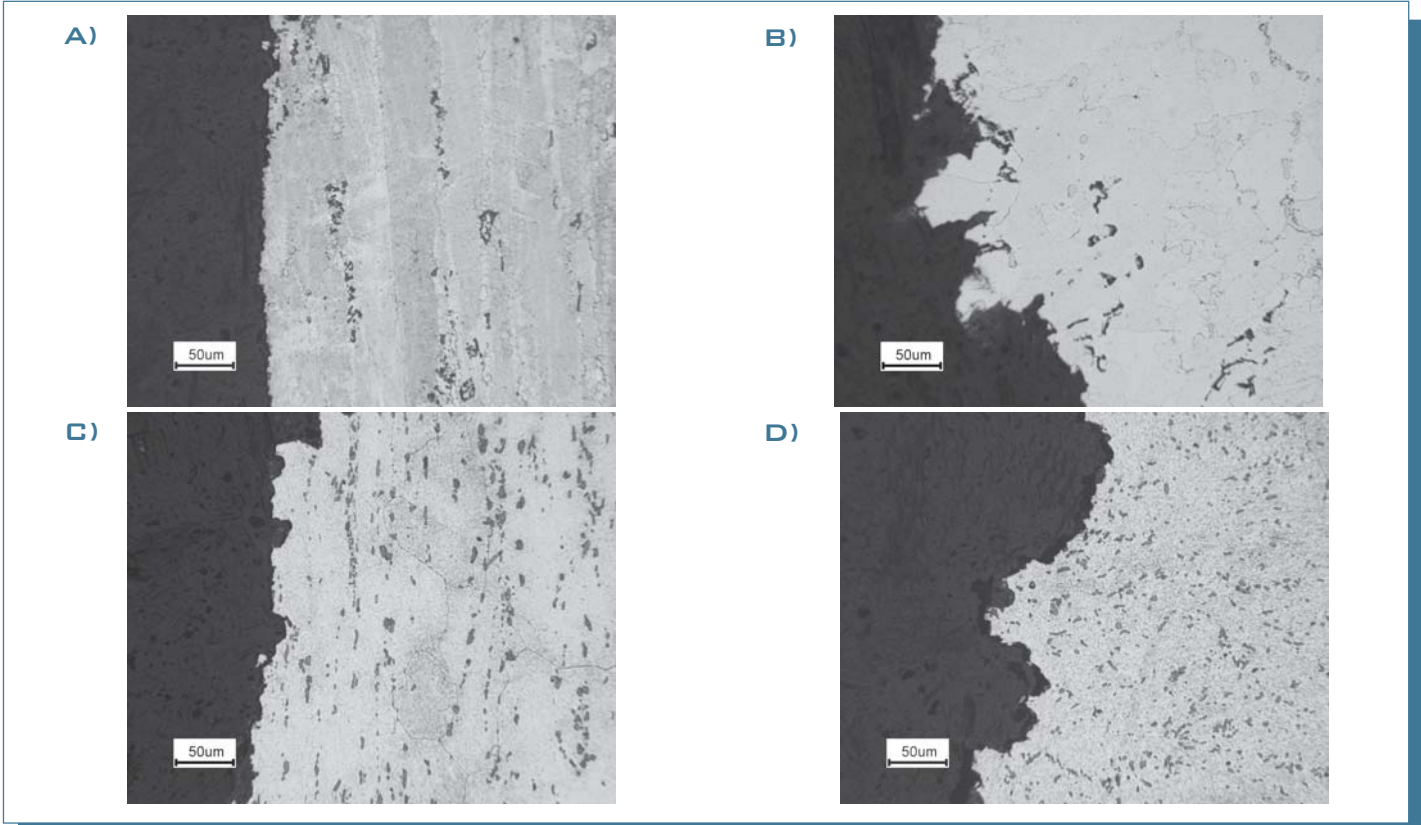

Fig. 6: Microstructure in the region of unstable crack propagation on longitudinal section of CT specimens. a) 2014-A forging, CL direction; b) 2014-B forging, CL direction; c) and d) 2618 forging, CL and CR directions, respectively.
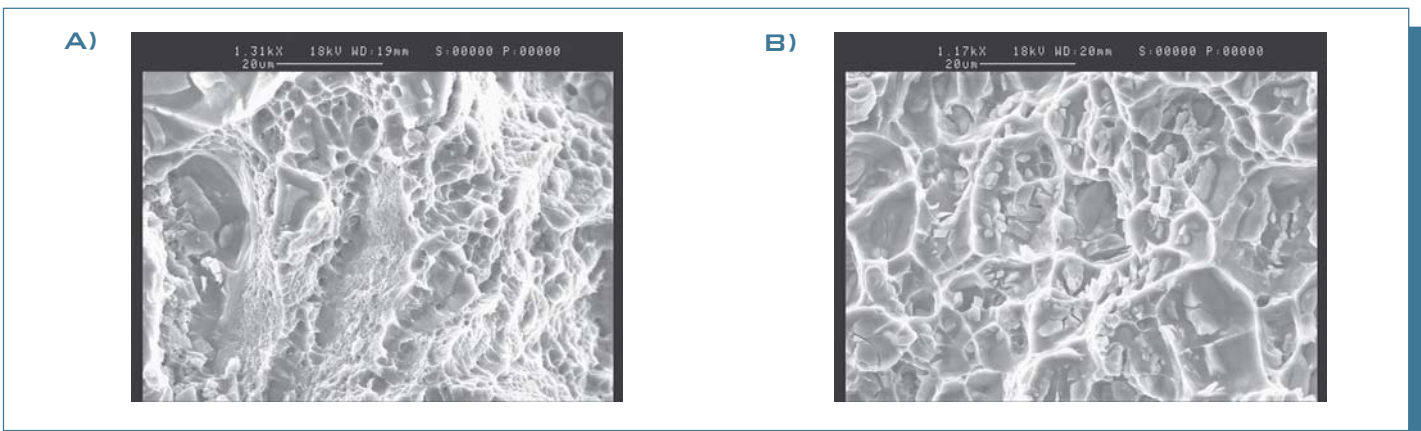

Fig. 7: Fracture surface sampled in CL direction of 2014-B forging (a) and of 2618 forging (b) tested at room temperature.
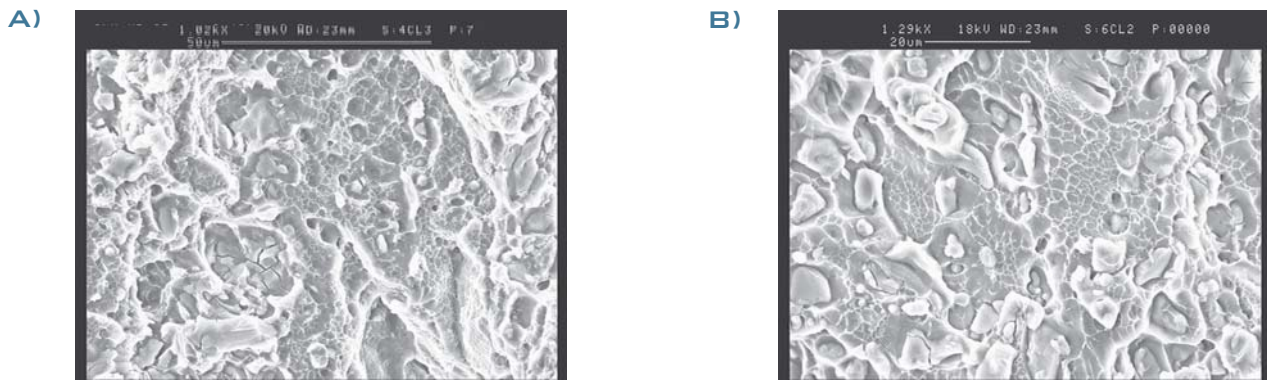
Fig. 8: Fracture surface of cracks propagated at 130°C in specimen with CL orientation of 2014-A (a) and 2618 (b) forgings.

4. DISCUSSION

In the examined forgings crack propagated in a ductile manner, in some cases by an intergranular ductile mode, linking the early fractured coarse intermetallic particles, located at inter or intragranular position in the different materials investigated.

Following the approach proposed by Hahn and Rosenfield [2] for aluminium alloys, it can be stated that crack propagates when the size of extensive plastic strain formed ahead of the crack tip corresponds to the average coarse interparticle distance (δ) Further, according to these authors, K and d are correlated as follows:

$$\delta =(0.5K^2)/(E \bullet YS) \qquad (5)$$

In the case of 2618 forging the δ values estimated using room temperature tensile and toughness properties were 11 and 15 μm for specimen orientations CL and CR, respectively, comparable to the average interparticle size between the intragranular particles (mainly $FeNiAl_9$ particles) in longitudinal and radial direction, respectively. The preferred particle orientation and their tendency to align axially in the forging regions where specimens were sampled corresponds to a greater interparticle distance in the crack propagation direction of CR specimens. As previously presented, in the specimens obtained from forgings made of AA2014 alloy the crack proceeds in a ductile manner but along an intergranular path, intercepting the oriented coarse aligned intermetallic particles axially. The values of δ computed from equation 5 for these two forgings are 6.7 and 9 μm for CL and CR specimen of 2014-A forging, respectively. In the case of the last forging (2014-B), δ equals 12 μm for both CL and CR directions. Thus, also in the case of AA2014 alloy, d is comparable to the interparticle distance along the crack path. It can be thus stated that fracture toughness is correlated to the mean interparticle distance along the crack path.

The above observations well agree with the simple correlation proposed by Hahn and Rosenfield [2] for the case of forged Al-alloy parts (where fracture is initiated by cracking of large intermetallic particles once reached critical stress/strain levels in the region of extensive deformation at the crack tip [3]) and fracture toughness is correlated to the mean interparticle distance along the crack path.

Thus, forgings of the same heat treatable alloy, even in the same heat treatment condition and with comparable hardness and tensile properties can show significantly different fracture behaviour, depending on intermetallic particle population. Especially, as the mean interparticle distance along the crack path between the coarser intermetallic particles increases, the nucleation of voids at these particles is shifted at higher applied loads and toughness is improved.

The role of coarse intermetallic particles and the need to reduce their amount, to optimize their size and distribution in forgings (taking into account the most critical crack propagation directions in the components) in order to increase material toughness is therefore highlighted.

CONCLUSIONS

The toughness properties in opening mode I of forgings made of AA2014 and AA2618 aluminium alloys with different microstrctural conditions were presented.

Fracture toughness ranged between 19 and 26 MPam^0.5 , depending on the material and specimen direction. Fracture toughness was in general lower for specimen sampled in CL direction. In the examined forgings crack propagated in ductile manner, in some cases by an intergranular ductile mode, linking in any case the voids formed at the early fractured inter- or intragranular coarse intermetallic particles. No significant difference in toughness nor in the fracture mode was observed when tests were performed at room temperature or at 130°C.

Fracture toughness properties were related to the presence and distribution of the coarse intermetallic phases within grains or at their boundaries in the different investigated alloys.

The simple correlation proposed by Hahn and Rosenfield between fracture toughness and the mean interparticle size was found to be applicable when the interparticle distance along the crack path (different for different sampling direction in forgings where these particle were aligned along flow directions) is taken into account. An observation and quantitative assessment of the distribution of coarse intermetallic phases on optical micrographs can be a useful tool to check fracture toughness properties of different forgings in their peak aged condition when yield strength is known.

REFERENCES

[1] J.S. Robinson, R.L. Cudd, J.T. Evans. Creep resistant aluminium alloys and their applications. Material Science and Technology, 19 (2003) pp. 143-155.

[2] G.T. Hahn, A.R. Rosenfield. Metallurgical Factors Affecting Fracture Toughness of Aluminum Alloys. Metall. Trans. A, (1975) pp. 653-668.

[3] T. Kobayashi. Strength and fracture of aluminium alloys. Materials Science Engineering, A286 (2000) pp. 333-341.

[4] A.P. Reynolds, E.P. Crooks. The effect of thermal exposure on the fracture behaviour of aluminium alloys intended for elevated temperature service. in "Elevated temperature on fatigue and fracture", ASTM STP 1297. Williamsbourg, Virginia(USA), (1997) 191-205.

[5] B.Q. Li, A.P. Reynolds. Correlation of grain-boundaries precipitates parameters with fracture youghness in an Al-Cu-Mg-Ag alloy subjected to long-term thermal exposure. Journal of Materials Science, 33 (1998) pp. 5849-5853.

[6] ASTM B 645-02 Practice for plane-strain fracture toughness testing of aluminium alloys.

[7] ASTM E 399-99 Standard test method for plane-strain fracture toughness of metallic materials.

[8] ASTM E1820-01. Standard test method for measurement of fracture toughness.